

**Normal-deformed structures in hafnium isotopes**H. Taheri,<sup>1</sup> A. Kardan,<sup>2,\*</sup> and M. H. Hadizadeh Yazdi<sup>1,†</sup><sup>1</sup>*Department of Physics, Ferdowsi University of Mashhad, Mashhad, Iran*<sup>2</sup>*School of Physics, Damghan University, Damghan, Iran*

(Received 9 May 2018; revised manuscript received 4 September 2018; published 19 November 2018)

The structures of yrast normal-deformed (ND) bands in Hf isotopes have been investigated using the unpaired cranked Nilsson-Strutinsky (CNS), and the paired cranked Nilsson-Strutinsky-Bogoliubov (CNSB) models. New optimized Nilsson parameters have been derived and used in the models to interpret the experimental data in <sup>168–175</sup>Hf isotopes. The calculated kinematic moments of inertia, as well as the excitation energies of the yrast bands, have been compared with the experimental findings, and good agreements are observed. Configuration changes along the yrast lines have been traced by the aid of the CNS calculations. The calculated single-particle excitations shed more light on the nature of the crossings and successfully explain some features of the observed rotational bands which had not been clear before.

DOI: [10.1103/PhysRevC.98.054313](https://doi.org/10.1103/PhysRevC.98.054313)**I. INTRODUCTION**

In the  $A \approx 160$  mass region, highly deformed shapes have been well established for nuclei [1]. In this region, Hf isotopes have been extensively investigated, and a variety of minima, from normal-deformed (ND) to strongly deformed (SD), including triaxial strongly deformed (TSD) shapes, have been predicted [2–7]. The interplay between collective motion and single-particle excitations introduces special features in the high-spin structure of deformed nuclei. Considerable theoretical efforts have revealed the deformation and single-particle properties of these nuclei at high rotational states, which include microscopic approaches, such as relativistic mean-field theory [8,9] or relativistic Hartree-Bogoliubov formalism [10,11], and macroscopic-microscopic approaches, such as cranked Nilsson-Strutinsky (CNS) [12,13] or cranked shell models (CSM) [14–16]. A known important residual interaction in nuclei is the pairing correlation, which has striking effects on the rotational bands' behavior, especially in the low-spin region. For example, the well-known back-bending effect is now well established to be due to the pairing forces [15,17]. In general, the complexity due to the mixing of the states near the Fermi level, as a result of the pairing field, makes it more difficult to describe the rotating nuclei [16]. Hence, in most formalisms which include pairing, only yrast states can be calculated, and neither single-particle excitations nor configuration changes can be deduced as a comparable outcome. So, paired formalisms, in spite of being generally successful in reproducing crossing frequencies and aligned angular momenta at low or medium rotational frequencies, have deficiencies in treating the crossings if they are due to configuration changes. On the other hand, by neglecting the pairing, which is done in the CNS model, a more transparent

description of single-particle energies can be given. In the CNS formalism, in the absence of the pairing and because of the simplicity of the modified oscillator potential, it is possible to trace excited configurations, in addition to the yrast states, by fixing the number of particles in different  $j$  shells or group of  $j$  shells. Studies for <sup>161</sup>Lu show that at spin values above the neutron  $i_{13/2}$  and the proton  $h_{11/2}$  band crossings ( $I > 30$ ), the relative energies of different bands are described rather well by the unpaired CNS calculations [18]. However, specifically at low spins, this formalism suffers from the absence of the pairing, and the calculations show rather high discrepancies with the experimental data; see, for example, Refs. [19–21]. Using paired and unpaired formalisms in parallel should lessen the deficiencies to some extent. In this work, we study the structures of the yrast ND bands of several Hf isotopes by using the CNS calculations to trace the configuration changes along the yrast lines calculated by the CNSB (cranked Nilsson-Strutinsky-Bogoliubov) model [22], which has the same basis as the CNS model plus the pairing. We first try to derive a set of new parameters for the models which reproduce the observed features of the Hf isotopes better than the so-called standard parameters.

**II. COMPARISON BETWEEN CNS AND CNSB FORMALISMS**

In the CNS formalism, the Hamiltonian is taken as

$$H = h_{\text{MO}}(\varepsilon_2, \gamma, \varepsilon_4) - \omega j_x, \quad (1)$$

where  $h_{\text{MO}}$  denotes the modified oscillator potential and  $\omega j_x$  is the cranking term around the principal  $x$  axis. The total energies are minimized with respect to deformation parameters ( $\varepsilon_2, \gamma, \varepsilon_4$ ) at each spin (frequency) value. Neglecting the pairing correlations, along with some off-shell elements of the Hamiltonian matrix [19], makes it possible to separate the orbitals in each  $N$  shell into high- $j$  and low- $j$  groups. Thus, the configurations can be specified not only by the number

\*aakardan@du.ac.ir

†Corresponding author: mhhadi@um.ac.ir

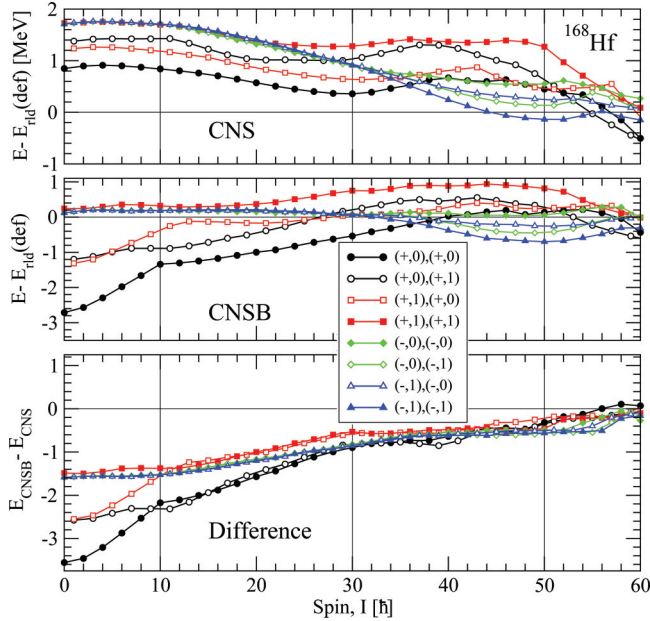


FIG. 1. Top panel: Unpaired CNS energies. Middle panel: Paired CNSB energies. Lower panel: Their differences for positive-parity yrast configurations in  $^{168}\text{Hf}$  (excitation energies are plotted relative to a rotating liquid drop reference).

of particles in the orbitals of different parity and signature, but also by the number of particles in these two groups in different  $N$  shells. Consequently, a large number of different configurations in the yrast region can be determined.

In the CNSB formalism, the same potential as in the CNS model, plus a pairing term, is used,

$$H = h_{\text{MO}}(\varepsilon_2, \gamma, \varepsilon_4) - \omega j_x - \Delta(P^\dagger + P) - \lambda \hat{N}, \quad (2)$$

where  $P^\dagger(P)$  is the pair creation (annihilation) operator and  $\hat{N}$  is the particle number operator. The total energies, after adapting the particle-number projection and the Strutinsky renormalization, are minimized with respect to  $\Delta$  (pairing gap) and  $\lambda$  (Fermi level), as well as the deformation parameters. By fixing parity  $\pi$  and signature  $\alpha$  for protons and neutrons separately, in total, 16 combinations of the form  $(\pi, \alpha)_p(\pi, \alpha)_n$  can be configured (for simplicity, hereafter, subscripts  $p$  and  $n$  will be omitted in the captions and in the text). The total energies in both the CNS and the CNSB are obtained through the Strutinsky renormalization method [23,24], as a sum of the rotating liquid drop ( $E_{\text{RLD}}$ ) and the shell energies. The same  $E_{\text{RLD}}$ , calculated in the Lublin-Strasbourg model [25], and same parameters are used in the both cases. This makes it possible to compare the results of the two formalisms directly. According to the Hamiltonians, the only difference between the CNS and the CNSB yrast configurations is the pairing energy. The comparison of the paired and unpaired results for the positive-parity bands of  $^{168}\text{Hf}$  are presented in Fig. 1. In the top panels of Fig. 1, the excitation energies relative to those of a rotating liquid drop are plotted as functions of spin and, in the lower panel, the energy differences (pairing energies) are illustrated. It is seen that the pairing energies have almost the same trend

for the different configurations and also have very small and fixed values for  $I > 50$ . Some discontinuities are seen in these differences, especially at  $I \approx 10$  and  $I \approx 30$ , which should correspond to the paired crossings.

The CNS configurations in the text are labeled according to the number of particles in the high- $j$  and low- $j$  orbitals of the last-filled  $N$  shells, as

$$\pi(h_{11/2})^{p_1}(h_{9/2}f_{7/2})^{p_2}(i_{13/2})^{p_3},$$

$$\nu(i_{13/2})^{n_1}(i_{11/2}g_{9/2})^{n_2}(j_{15/2})^{n_3}$$

or

$$[p_1(p_2p_3), n_1(n_2n_3)],$$

in short notation (the numbers in the parentheses are omitted when they are equal to zero).

### III. NEW NILSSON PARAMETERS FOR $N = 4, 5, \text{ AND } 6$ SHELLS

For Hf isotopes, the standard Nilsson parameters [12] are used in the CNS and the CNSB formalisms. This set of parameters is introduced as an appropriate set for the well-deformed nuclei in the rare-earth-metal region [19]. Comparing experimental and calculated quantities, such as crossing positions, excitation energies, and parity-signature sequences of the lowest bands gives the opportunity to optimize these parameters. The active shells in the Hf mass region are  $N = 4, 5, \text{ and } 6$ , and therefore the Nilsson parameters for protons and neutrons of these shells can be adjusted so that the calculated and the observed results would match as much as possible. For example, the crossing between the configurations assigned to bands 1 and 3 in  $^{168}\text{Hf}$  [19] ([8,4] and [8,5], respectively) occurs due to the crossing of the  $5/2[523]$  and  $5/2[642]$  levels at  $\hbar\omega \approx 0.85$  MeV with the standard levels; see Fig. 2, in

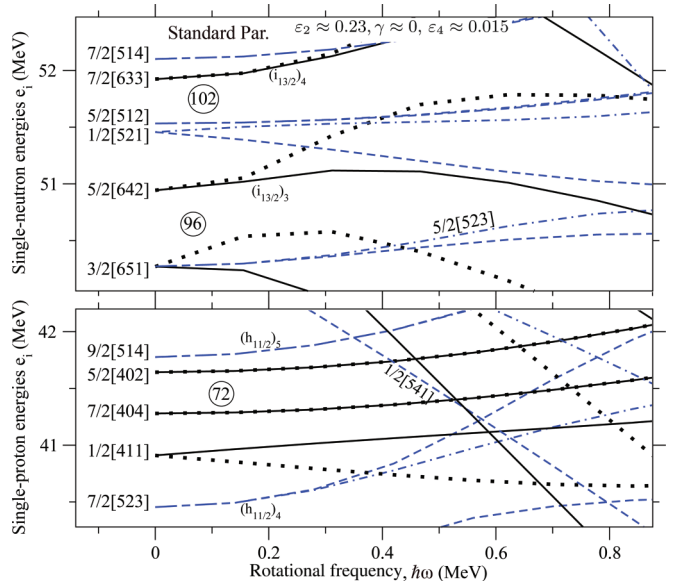
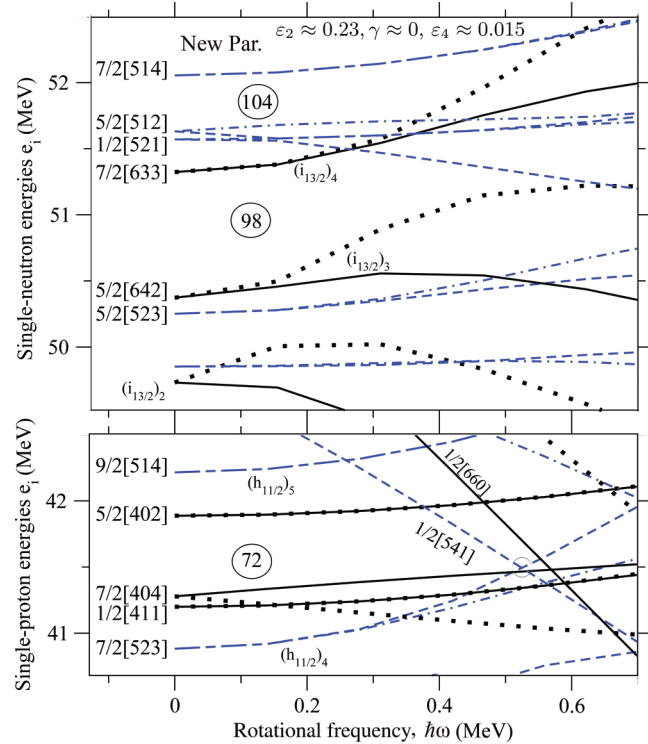
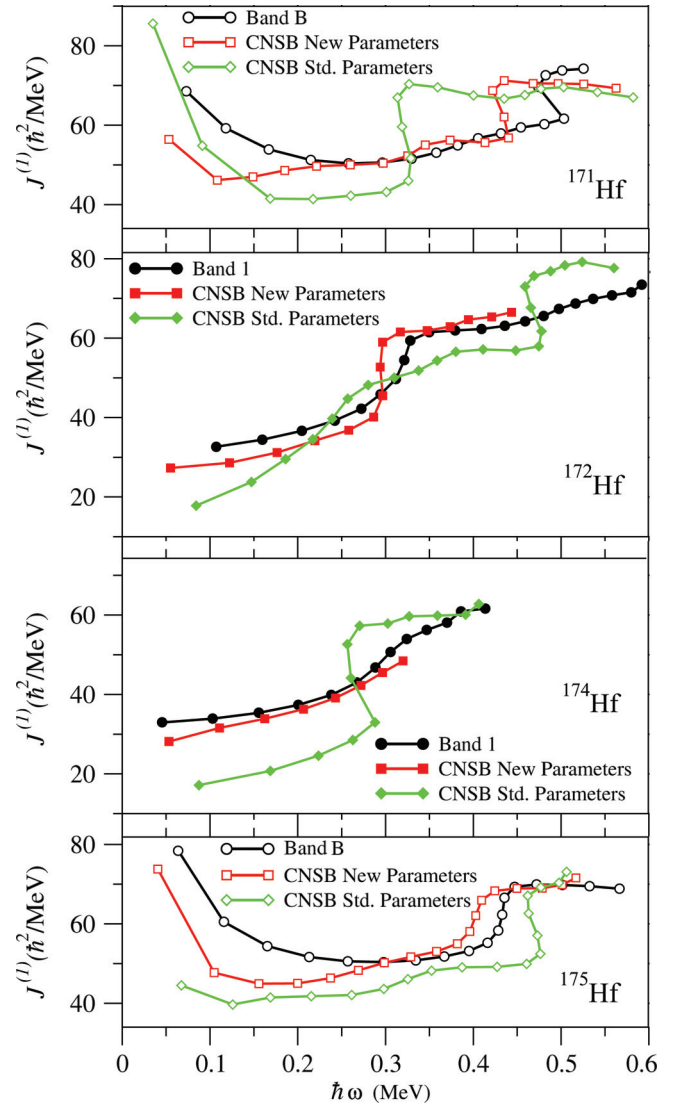


FIG. 2. Top panel: Single-neutron energies. Lower panel: Single-proton energies as functions of rotational frequency using the standard parameters at the deformation  $\varepsilon_2 \approx 0.23, \gamma \approx 0$ , and  $\varepsilon_4 \approx 0.015$ .

TABLE I. Standard and new  $\kappa$ - $\mu$  parameters for  $N = 4, 5$ , and 6 proton and neutron shells.

		$\kappa_{\text{old}}$	$\mu_{\text{old}}$	$\kappa_{\text{new}}$	$\mu_{\text{new}}$
$N = 4$	Protons	0.065	0.570	0.0702	0.6156
	Neutrons	0.070	0.390	0.0728	0.4056
$N = 5$	Protons	0.060	0.650	0.0564	0.6110
	Neutrons	0.062	0.430	0.0645	0.4472
$N = 6$	Protons	0.054	0.690	0.0524	0.6693
	Neutrons	0.062	0.340	0.0670	0.3672

which the single-particle energies using standard parameters are plotted versus frequency at the deformation parameters expected for normal deformations;  $\varepsilon_2 \approx 0.23$  and  $\gamma \approx 0$ . Experimentally, bands 1 and 3 cross at  $\hbar\omega \approx 0.5$  MeV ( $I = 36$ ) (see Fig. 11 in Ref. [19]), indicating that the gap between the aforementioned levels in the standard scheme must be decreased. This can be done by lowering the  $i_{13/2}$  levels by increasing  $\kappa$ - $\mu$  parameters for  $N = 6$  neutrons. Naturally, other levels must be adjusted so that the calculated total energies do not change unexpectedly. Best-fitted parameters, with all factors taken into account, are obtained for Hf isotopes and reported in Table I. In Fig. 3, new single-particle levels at the deformation  $\varepsilon_2 \approx 0.23$ ,  $\gamma \approx 0$ , and  $\varepsilon_4 \approx 0.015$  are shown. In the CNSB calculations, the pairing strength,  $G$ , is also adjusted to reproduce the experimental energy trends better.


 FIG. 3. Top panel: Single-neutron energies. Lower panel: Single-proton energies as functions of rotational frequency using new parameters at the deformation  $\varepsilon_2 \approx 0.23$ ,  $\gamma \approx 0$ , and  $\varepsilon_4 \approx 0.015$ .

 FIG. 4. Calculated kinematic moments of inertia,  $J^{(1)}$ , of some yrast bands in Hf isotopes using standard (Std.) and new parameters along with the experimental values versus frequency.

It is found that for heavier isotopes,  $G$  must be lowered more compared to the standard prescription in the CNSB code [26]. The values 0.95 and 0.88 have been used for  $^{168-170}\text{Hf}$  and  $^{171-175}\text{Hf}$ , respectively. In Fig. 4, the calculated moments of inertia,  $J^{(1)}$ , using both the new and standard parameters, for cases most affected by adjusting the parameters, are compared. It is seen that the agreement between the calculated and the experimental results is noticeably improved by the new parameters.

#### IV. YRAST ND BANDS IN HF ISOTOPES

A close look at the single-particle energies in Fig. 3 shows that a large gap exists for  $Z = 72$  up to  $\hbar\omega \approx 0.5$  MeV that makes  $\pi(N = 4)^{-6}(h_{11/2})^8$  configuration a favored proton configuration in this frequency range for yrast bands in Hf isotopes. Beyond  $\hbar\omega \approx 0.5$  MeV, the  $1/2[541]$  level falls below the  $7/2[523]$  level, while the signature parity is preserved.

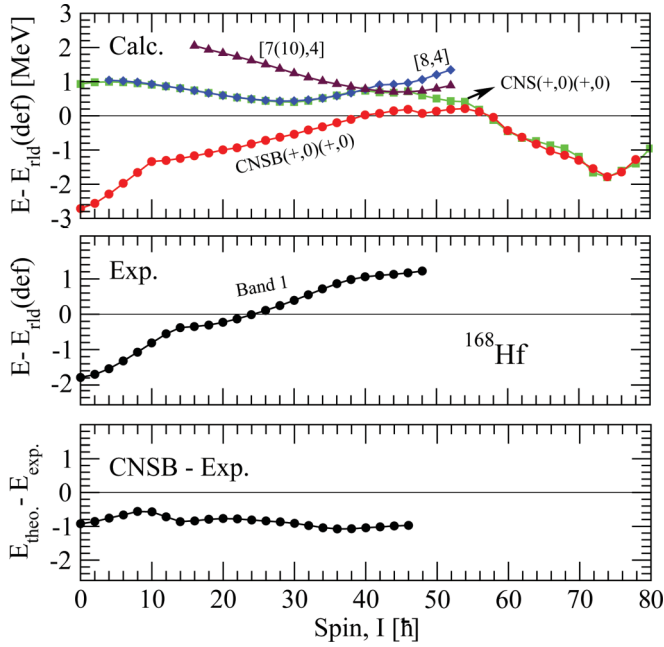


FIG. 5. Top panel: Calculated paired and unpaired yrast bands. Middle panel: Experimental band in  $^{168}\text{Hf}$  (excitation energies are calculated relative to a rotating liquid drop energy reference). Lower panel: Calculated paired (CNSB) and experimental energy differences.

Therefore, the  $\pi(N=4)^{-6}(h_{11/2})^7(h_{9/2}f_{7/2})^1$  configuration is favored at higher frequencies. This level crossing corresponds to the crossings observed at high frequencies in most ND bands that cannot be calculated directly in paired formalisms. In comparison with the standard parameters (Fig. 2), there is a larger gap for  $Z=72$  with the new parameters, and also the proton level crossings show better agreement with the experiments. In what follows, the structure of the yrast ND bands of  $^{168-175}\text{Hf}$  isotopes are discussed utilizing the new parameters in the CNS and the CNSB formalisms.

### A. Band 1 in $^{168}\text{Hf}$

Configuration changes along the yrast lines of the Hf isotopes are determined in the CNS formalism, as shown in Fig. 5 (top panel) for the  $(+,0)(+,0)$  state of  $^{168}\text{Hf}$ . Comparison of the yrast lines calculated in the CNS and CNSB frameworks shows the effect of pairing correlations clearly. One can see that the lines meet at  $I \approx 50$  and continue the same trends afterward, where pairing almost vanishes at high spins. Both energy trends show same discontinuities where the configuration changes. Furthermore, the CNSB energies display more discontinuities due to the pair alignments. Thus, one can assess whether the crossings along the rotational bands appear due to pair alignments or structural changes by comparing the calculated yrast lines in the paired and unpaired formalisms.

The top panel of Fig. 5 demonstrates the paired and unpaired calculated positive-parity yrast bands of  $^{168}\text{Hf}$ . In the figures, excitation energies are drawn relative to a liquid drop energy reference as a function of spin. As one can see,

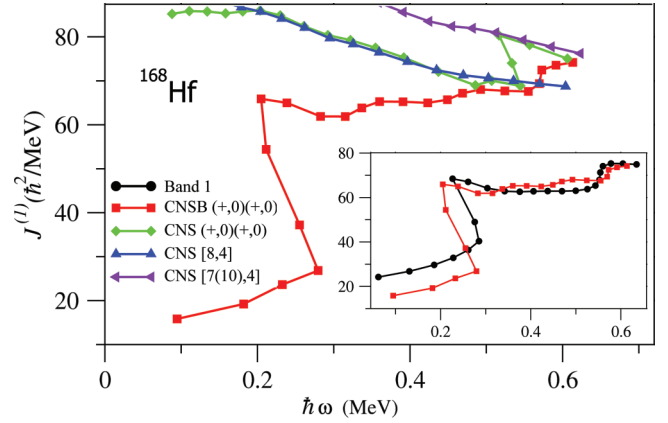


FIG. 6. Calculated kinematic moments of inertia,  $J^{(1)}$ , for bands in Fig. 5. Inset compares the experimental and paired CNSB  $J^{(1)}$ s.

the yrast band has the configuration  $[8,4] [\pi(h_{11/2})^8 \nu(i_{13/2})^4]$  up to  $I \approx 40$  and  $[7(10),4] [\pi(h_{11/2})^7 (h_{9/2}f_{7/2})^1 \nu(i_{13/2})^4]$  for higher spins. The calculated configuration deformations are  $\varepsilon_2 \approx 0.22$ ,  $\gamma \approx -2$  and  $\varepsilon_2 \approx 0.23$ ,  $\gamma \approx 0$ , respectively. The middle panel of Fig. 5 displays the experimental yrast band [7], and in the lower panel, the experimental and the calculated paired (CNSB) bands are compared by the illustration of their difference. The fairly constant differences at the value of approximately  $-1$  MeV indicate good agreement between the theory and the experiment. The first alignment in band 1 is a paired crossing which occurs at  $\hbar\omega \approx 0.26$  MeV, in the region of the  $[8,4]$  configuration, which is not seen in the CNS calculations. This alignment, observed systematically in  $N=96$  nuclides, such as  $^{167}\text{Lu}$  [27],  $^{169}\text{Ta}$  [28], and  $^{170}\text{W}$  [29], causes a back-bending in the moments of inertia curves. This back-bending is nicely reproduced by the paired calculations; see Fig. 6. A second discontinuity in the rotational pattern occurs when the configuration changes from  $[8,4]$  to  $[7(10),4]$  at  $I \approx 40$  ( $\hbar\omega \approx 0.55$  MeV). The same discontinuity can be seen in both the paired and unpaired trends at the observed frequency. Figure 6 indicates this discontinuity in the moments of inertia pictures, where the CNS  $J^{(1)}$  trend jumps from  $[8,4]$  to  $[7(10),4]$  configuration. In the inset of Fig. 6, the experimental and calculated  $J^{(1)}$ s are also compared. As one can see, the experimental and the paired and unpaired calculated crossings occur at almost the same frequencies.

### B. Bands A and B in $^{169}\text{Hf}$

In the ground state of  $^{169}\text{Hf}$ , the last odd neutron occupies the third  $i_{13/2}$  level ( $5/2[642]$ ), which has a large signature splitting; see Fig. 3. Thus, the suggested configuration for the ground band would be  $[8,5], \pi(h_{11/2})^8 \nu(i_{13/2})^5$ . The absence of a back-bending at low spins in bands A and B explains the odd neutron number on the  $i_{13/2}$  orbitals. The calculated deformation for both signatures is  $\varepsilon_2 \approx 0.23$ ,  $\gamma \approx -5$ . In the top panel of Fig. 7, the calculated yrast bands for  $^{169}\text{Hf}$  are shown. As can be seen, the calculated signature splitting of the  $[8,5]$  configuration is consistent with those of the yrast bands A and B [30], which are shown in the middle panel. The differences of the CNSB energies with the experimental

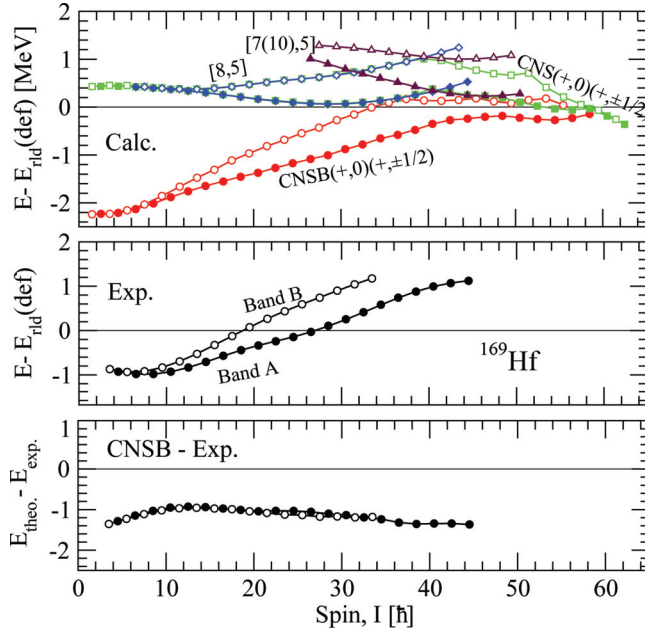


FIG. 7. Top panel: Calculated paired and unpaired yrast bands. Middle panel: Experimental bands A and B in  $^{169}\text{Hf}$  (excitation energies are calculated relative to a rotating liquid drop energy reference). Lower panel: Paired (CNSB) and experimental energy differences. Solid symbols correspond to signature  $\alpha = 1/2$  and open symbols to signature  $\alpha = -1/2$ .

ones are seen in the lower panel of Fig. 7, which are fairly constant at  $\approx -1$  MeV. Band A is observed up to  $I = 89/2$  and band B up to  $I = 67/2$ .

The former, as can be seen from the CNS trends, changes its configuration to  $[7(10), 5]_{\alpha=1/2}$  with the deformation  $\varepsilon_2 \approx 0.24$ ,  $\gamma \approx -3$  at  $I = 81/2$  ( $\hbar\omega \approx 0.56$  MeV), where the second crossing is observed. A second crossing due to configuration change is also predicted for band B at about the same spin as band A.

### C. Band 1 in $^{170}\text{Hf}$

Band 1 is the positive-parity yrast band in  $^{170}\text{Hf}$  [2]. In the ground state of  $^{170}\text{Hf}$ , the third  $i_{13/2}$  level (Fig. 3) is full and thus the  $[8,6]$  configuration has the same parity and signature as band 1. This configuration is preserved as yrast, up to the last reported spin of band 1,  $I = 40$  ( $\hbar\omega \approx 0.56$  MeV), and then changes to  $[7(10),6]$ , where the observed band shows the beginning of an up-bending. The calculated deformations are  $\varepsilon_2 \approx 0.23$ ,  $\gamma \approx -7$  and  $\varepsilon_2 \approx 0.24$ ,  $\gamma \approx -3$ , respectively. The corresponding bands are shown in Fig. 8. The illustration in the lower panel of Fig. 8 demonstrates that the calculated band reproduces the observed energy trend completely, although at  $\approx 1$  MeV lower in energy. The crossing frequency of  $\hbar\omega \approx 0.27$  MeV and the gain in the moment of inertia due to the paired alignment is well reproduced by the paired calculations (not shown). The up-bending at the end of the band is also reproduced by the unpaired configuration change at the right frequency.

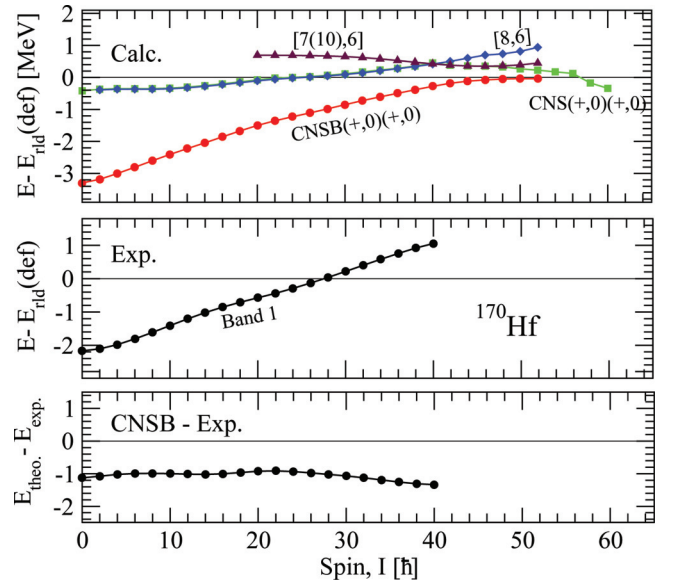


FIG. 8. Top panel: Calculated paired and unpaired yrast bands. Middle panel: Experimental band 1 in  $^{170}\text{Hf}$  (excitation energies are calculated relative to a rotating liquid drop energy reference). Lower panel: Paired (CNSB) and experimental energy differences.

### D. Bands A and B in $^{171}\text{Hf}$

According to the single-particle energies in Fig. 3, the odd neutron will occupy the fourth  $i_{13/2}$  level in the lowest energy states in  $^{171}\text{Hf}$ . The two resulting positive-parity signature-partner bands are consistent with the lowest observed bands, A and B, in  $^{171}\text{Hf}$  [31]; see Fig. 9. As seen in the top panel of Fig. 9, the positive-signature band has the configuration  $[8, 7]_{\alpha=1/2}$  ( $\varepsilon_2 \approx 0.23$ ,  $\gamma \approx -8$ ) up to  $I \approx 79/2$ , and  $[7(10),7]$  ( $\varepsilon_2 \approx 0.25$ ,  $\gamma \approx -4$ ) afterward. The other signature has the configuration  $[8, 7]_{\alpha=-1/2}$  ( $\varepsilon_2 \approx 0.23$ ,  $\gamma \approx -6$ ) up to  $I \approx 55/2$ , and  $[8,5]$  ( $\varepsilon_2 \approx 0.23$ ,  $\gamma \approx -4$ ) afterward.

The calculated  $J^{(1)}$  moments in the paired and unpaired formalisms are compared in the top panel of Fig. 10 for  $\alpha = 1/2$  and in the lower panel for  $\alpha = -1/2$ . The experimental and paired calculated results are compared in the insets. Band A shows a sharp increase in the moment of inertia at  $\hbar\omega \approx 0.38$  MeV. This is characteristic of positive-parity yrast bands in neighboring  $N = 99$  even- $Z$  nuclides, like  $^{169}\text{Yb}$  [32],  $^{173}\text{W}$  [33], and  $^{175}\text{Os}$  [34]. All these bands have very similar excitation energies and moments of inertia, indicating their similar structures. They have been attributed to the configuration  $7/2[633]$  in the previous studies ( $[8,7]$  in our notation). This assignment is consistent with our calculations with the new parameters. On the other hand, with the standard parameters, the  $5/2[642]$  configuration ( $[8,5]$ ) as a positive-parity yrast state should be assigned to bands A and B. It can be seen in Fig. 10 that the first crossing in bands A and B is reproduced by the paired calculations and the second crossing by both the paired and unpaired calculations. The first crossing in band B appears as a gradual increase in the moments of inertia, indicating a strong interaction between  $i_{13/2}$  orbitals [31]. The observed crossing at  $\hbar\omega \approx 0.55$  MeV in band A is predicted to be due to the configuration change

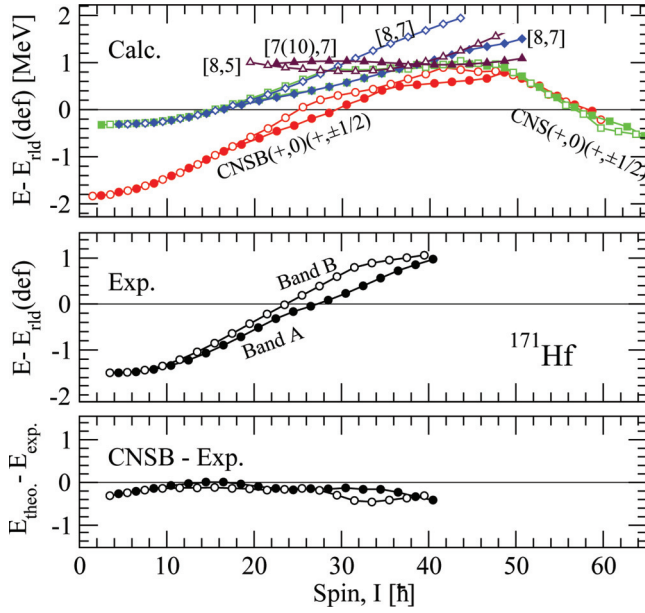


FIG. 9. Top panel: Calculated paired and unpaired yrast bands. Middle panel: Experimental bands A and B in  $^{171}\text{Hf}$  (excitation energies are calculated relative to a rotating liquid drop energy reference). Lower panel: Paired (CNSB) and experimental energy differences. Solid symbols correspond to signature  $\alpha = 1/2$ , and open symbols correspond to signature  $\alpha = -1/2$ .

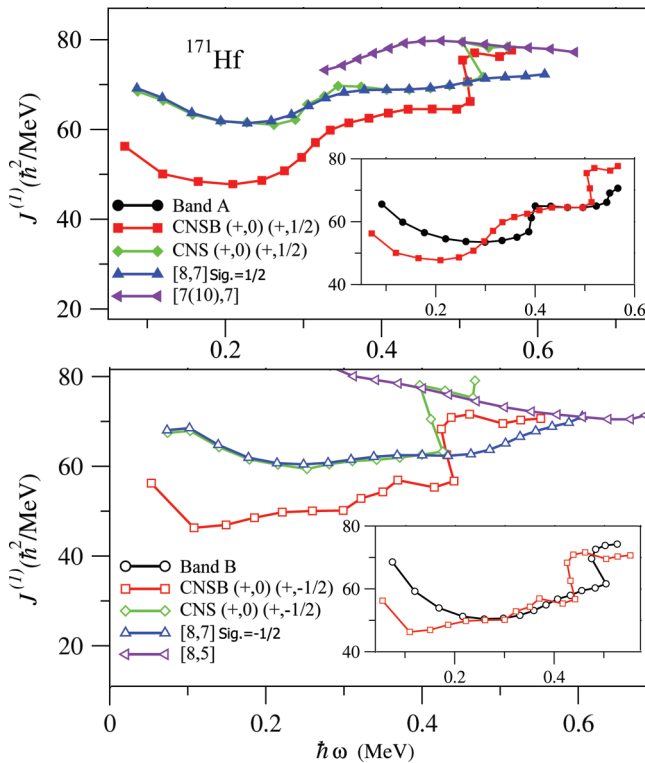


FIG. 10. Top panel: Calculated kinematic moments of inertia,  $J^{(1)}$ , of yrast bands in  $^{171}\text{Hf}$  for positive signature. Lower panel: Those for negative signature. Insets compare paired and experimental  $J^{(1)}$ s.

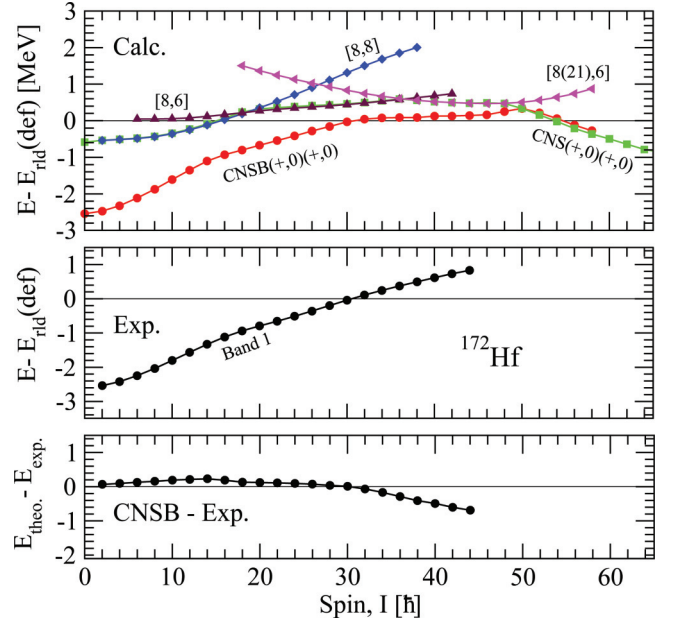


FIG. 11. Top panel: Calculated paired and unpaired yrast bands. Middle panel: Experimental band 1 in  $^{172}\text{Hf}$  (excitation energies are calculated relative to a rotating liquid drop energy reference). Lower panel: Paired (CNSB) and experimental energy differences.

to [7(10),7], i.e., due to the proton configuration change from  $\pi(h_{11/2})^8$  to  $\pi(h_{11/2})^7(h_{9/2}, f_{7/2})^1$ , which is also seen in other isotopes. On the other hand, the unpaired calculations predict a configuration change to [8,5], due to neutron excitations, for band B at  $I \approx 55/2$  ( $\hbar\omega \approx 0.45$  MeV). This configuration change reproduces the observed energy trend and the crossing at  $\hbar\omega \approx 0.5$  MeV as well, although at some lower frequencies. This is in contrast to the previous interpretation that this crossing is caused by proton alignments in Ref. [31].

### E. Band 1 in $^{172}\text{Hf}$

Band 1 with parity signature of (+,0) is yrast in  $^{172}\text{Hf}$  [35]. In  $^{172}\text{Hf}$ , the fourth  $i_{13/2}$  neutron level (Fig. 3), as Fermi surface, is full. The lowest-energy configurations, with parity signature of (+,0), which are calculated in the paired and unpaired formalisms, are displayed in Fig. 11 (top panel). It is seen that the yrast state has the configuration [8,8] ( $\epsilon_2 \approx 0.24$ ,  $\gamma \approx -7$ ) up to  $I = 18$  ( $\hbar\omega \approx 0.3$  MeV), and then it changes to [8,6] ( $\epsilon_2 \approx 0.23$ ,  $\gamma \approx -6$ ), where the last two neutrons are excited to the low- $j$  orbitals of the  $N = 5$  shell, at  $\hbar\omega \approx 0.3$  MeV (see Fig. 3). The [8,6] configuration is crossed by the [8(21),6] at  $I = 36$  ( $\hbar\omega \approx 0.47$  MeV). The calculated deformation of this last configuration is  $\epsilon_2 \approx 0.3$ ,  $\gamma \approx 3$ . Thus, practically, the configuration change from [8,6] to [8(21),6] is unexpected because of the large deformation change. As a result, band 1 should start with the configuration [8,8] and then continue with [8,6] up to high spins. This configuration change occurs at the frequencies where one expects the first neutron pair alignment. Thus, the observed crossing should be due to both features at the same time. As seen in Fig. 11 (lower panel), the differences between

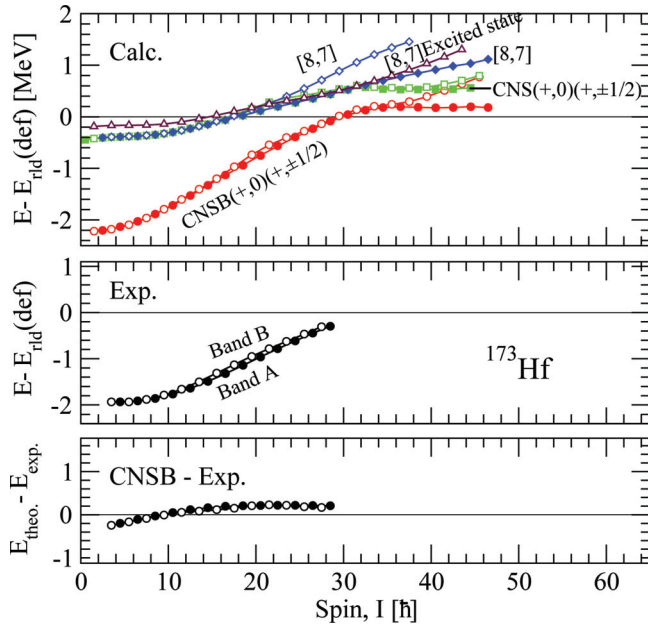


FIG. 12. Top panel: Calculated paired and unpaired yrast bands. Middle panel: Experimental bands A and B in  $^{173}\text{Hf}$  (excitation energies are calculated relative to a rotating liquid drop energy reference). Lower panel: Paired (CNSB) and experimental energy differences. Solid symbols correspond to signature  $\alpha = 1/2$ , and open symbols correspond to signature  $\alpha = -1/2$ .

the CNSB band and band 1 for different spins remain fairly unchanged at zero value.

### F. Bands A and B in $^{173}\text{Hf}$

In  $^{173}\text{Hf}$ , bands A and B (named 7/2[633] in Ref. [36]) are observed as positive-parity yrast bands, which have a narrow signature splitting. In this isotope, the low- $j$  1/2[521] and 5/2[512] neutron orbitals are located at the Fermi surface, with one particle occupancy (see Fig. 3). Thus, the ground states, in low frequencies, should have the [8,8] configuration with negative parity. This is consistent with the observed bands of  $^{173}\text{Hf}$ , where the ground states in the low frequencies have negative parity [36]. The [8,7] configuration, with positive parity, occurs if one neutron is excited from the fourth  $i_{13/2}$  to the 1/2[521] or 5/2[512] level. As indicated in Fig. 12 (top panel), the yrast bands have the configuration [8,7], while the negative-signature band changes to an excited [8,7] configuration at  $I = 43/2$ . This configuration change can be understood from the crossings that occur at  $\hbar\omega \approx 0.35$  MeV ( $I \approx 43/2$ ) in the single-particle levels (Fig. 3), where two neutrons transit from the  $7/2[633]_{\alpha=-1/2}$  to  $1/2[521]_{\alpha=1/2}$  and from the  $1/2[521]_{\alpha=-1/2}$  to  $7/2[633]_{\alpha=1/2}$  levels at the same time. The calculated configurations all have approximately the same deformation  $\varepsilon_2 \approx 0.24$ ,  $\gamma \approx -5$ . As can be seen in Fig. 12, the signature splitting and energy trends of the CNSB bands are well consistent with bands A and B. The aligned angular momenta  $i_x$  (alignment) of bands A and B are presented in the right panel of Fig. 13. The first paired alignment in these signature-partner bands occurs as a gradual increase in  $i_x$ , whereas the negative-signature band shows a

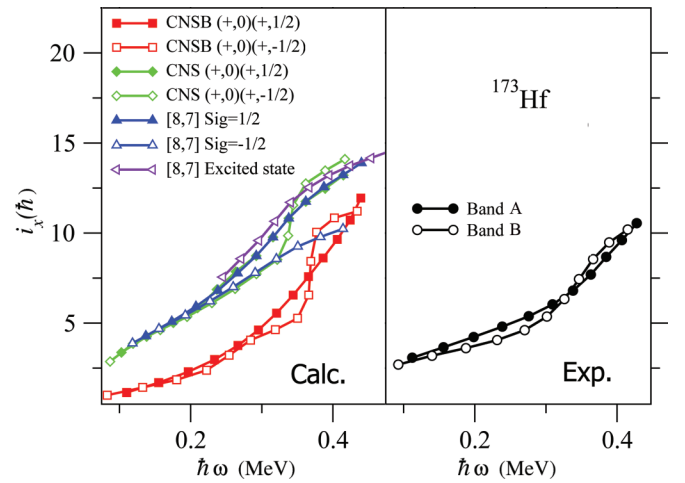


FIG. 13. Right panel: Aligned angular momenta (alignment),  $i_x$ , of bands A and B. Left panel: Those of paired and unpaired calculated bands in  $^{173}\text{Hf}$ .

slightly sharper crossing, causing its  $i_x$  to exceed that of the positive partner. The calculated alignments of the paired and unpaired bands are shown in the left panel of Fig. 13. One can see that the experimental alignments, especially their relative behavior, are well reproduced by the configuration change from [8,7] to the excited [8,7] in the negative-signature band.

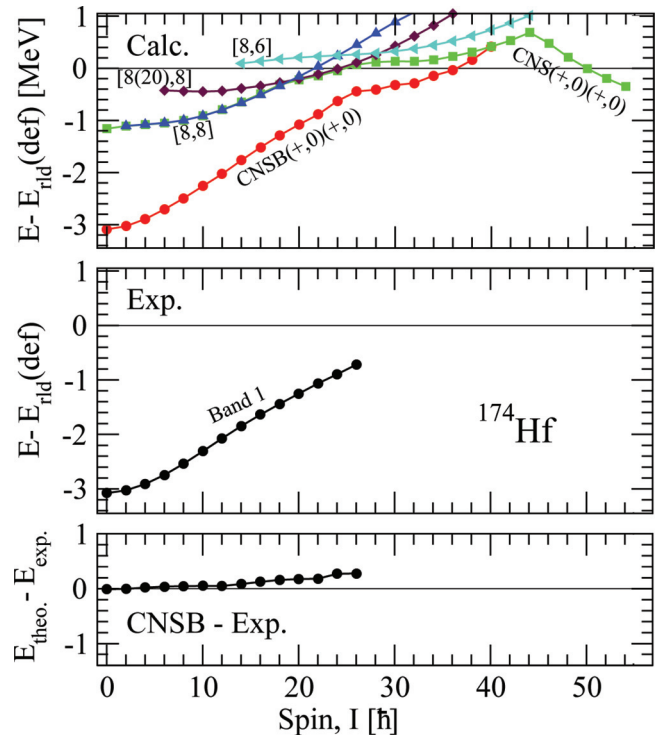


FIG. 14. Top panel: Calculated paired and unpaired yrast bands. Middle panel: Experimental band 1 in  $^{174}\text{Hf}$  (excitation energies are calculated relative to a rotating liquid drop energy reference). Lower panel: Paired (CNSB) and experimental energy differences.

### G. Band 1 in $^{174}\text{Hf}$

The positive-parity yrast band in  $^{174}\text{Hf}$  is band 1 [37], which has been observed up to  $I = 26$ . The lowest-energy bands with positive parity, calculated in the CNS and CNSB formalisms, are presented in Fig. 14 (top panel). As can be seen, the yrast line has the configuration [8,8] up to  $I = 18$  ( $\hbar\omega \approx 0.33$ ) and [8(20),8] afterward. The latter has the calculated deformation  $\varepsilon_2 \approx 0.3$ ,  $\gamma \approx 0$ , which is large in comparison with the [8,8] deformation ( $\varepsilon_2 \approx 0.24$ ,  $\gamma \approx -5$ ). This large deformation change is unexpected in practice and thus the [8,8] configuration should be assigned to band 1 up to high spins. As seen in the lower panel of Fig. 14, the differences between the calculated and experimental energies are well constant up to  $I = 18$ . At the highest observed spins,  $I \approx 24$  [8,8] is crossed by the [8,6] band, which has almost the same deformation as [8,8].

### H. Bands A and B in $^{175}\text{Hf}$

The signature-partner bands A and B, with a large signature splitting, are yrast among the positive-parity bands of  $^{175}\text{Hf}$  [6]. The signature splitting of the  $7/2[633]$  orbital at the vicinity of the Fermi surface of  $^{175}\text{Hf}$  (Fig. 3) indicates that it should correspond to bands A and B. The resulting [8,7] configuration, with the deformation  $\varepsilon_2 \approx 0.23$ ,  $\gamma \approx -5$  for both signatures, has been compared with the experimental

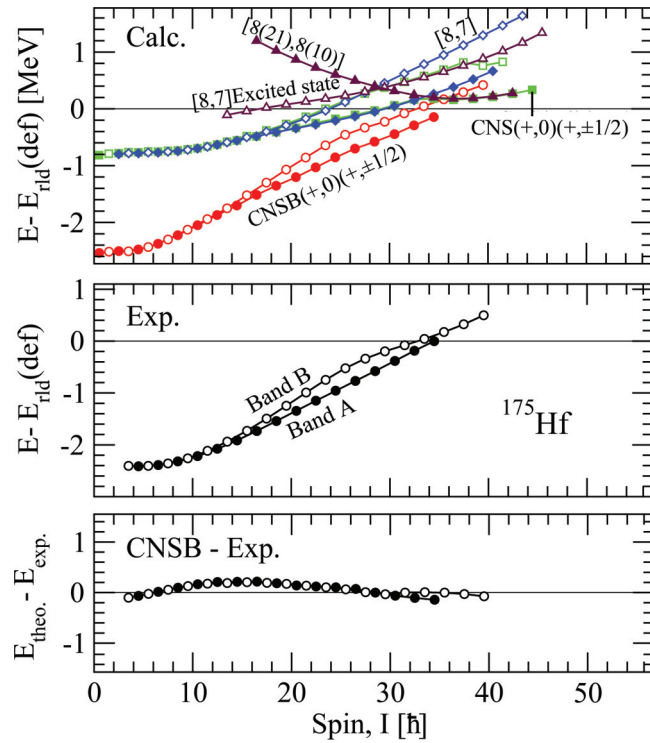


FIG. 15. Top panel: Calculated paired and unpaired yrast bands. Middle panel: Experimental bands A and B in  $^{175}\text{Hf}$  (excitation energies are calculated relative to a rotating liquid drop energy reference). Lower panel: Paired (CNSB) and experimental energy differences. Solid symbols correspond to signature  $\alpha = 1/2$  and open symbols correspond to signature  $\alpha = -1/2$ .

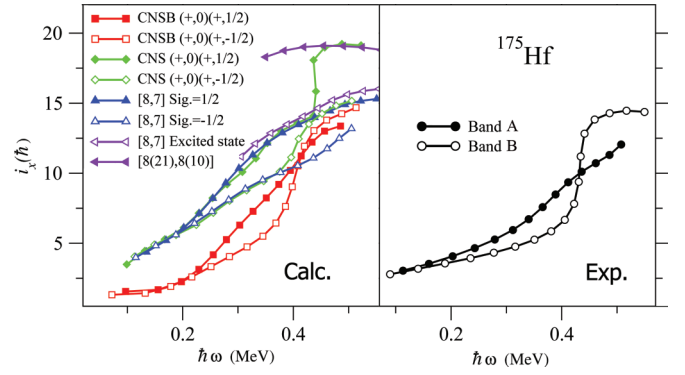


FIG. 16. Right panel: Aligned angular momenta (alignment),  $i_x$ , of bands A and B. Left panel: Those of paired and unpaired calculated bands in  $^{175}\text{Hf}$ .

bands in Fig. 15. The comparison of the paired bands with the experimental bands confirms that the signature splitting and the energies are well reproduced by the paired formalism. The experimental and the calculated alignments of bands A and B are presented in the right and left panels of Fig. 16, respectively. It is seen that the negative signature's alignments exceed the values in the positive one at  $\hbar\omega \approx 0.4$  MeV. As unpaired calculations show, there is a configuration change to an excited [8,7] configuration, with the deformation  $\varepsilon_2 \approx 0.23$ ,  $\gamma \approx -9$ , at  $I = 55/2$  ( $\hbar\omega \approx 0.4$  MeV) in the negative-signature partner; see Figs. 15 (top panel) and 16 (left panel). This is the neutron structure change which corresponds to the observed sharp crossing of the negative partner and explains well the odd relative behavior of the alignments of the two signature-partner bands (the same situation was discussed for  $^{173}\text{Hf}$ ). Configuration changes at low frequencies, such as what occur here, should explain the similar feature reported in some odd- $A$  neighboring isotones such as  $^{177,179}\text{Os}$  [38] and  $^{181,183}\text{Pt}$  [39,40]. At higher frequencies, there are configuration changes to [8(21),8(10)] ( $\varepsilon_2 \approx 0.32$ ,  $\gamma \approx 4$ ) for both signatures, which are practically unexpected because of the large deformation changes.

### V. CONCLUSION

We have revised the interpretation of the yrast ND band structures in several even-even and even-odd Hf isotopes assuming the unpaired CNS and the paired CNSB formalisms. While the previous configuration assignments are confirmed, more details about the configurations and also the origin of the crossings are obtained. By using the configuration-constrained CNS formalism, in parallel with the CNSB formalism, one would be able to identify configuration changes along the yrast lines.

We revised the previous assumptions about the nature of some crossings in Hf yrast bands which results in resolving some previous ambiguities. More specifically, the calculations reveal configuration changes in the negative signatures of the yrast bands of  $^{173,175}\text{Hf}$  at low frequencies, which explain rather well the observed different behavior in the alignments of the signature partner bands in odd- $A$  isotopes. This

feature, we believe, should also be the case for the neighboring odd- $A$  isotones. Furthermore, the observed crossing at high frequencies,  $\hbar\omega \approx 0.5$  MeV, in  $^{171}\text{Hf}$  is shown to be due to neutron single-particle excitation, while the crossings at  $\hbar\omega \approx 0.55$  MeV are due to proton excitations. Moreover, new Nilsson parameters are proposed for the models which reproduce the experimental results better than the standard parameters. In addition, we find that the pairing strength,  $G$ , must be decreased for heavier isotopes as 0.95 and 0.88 for  $^{168-170}\text{Hf}$  and  $^{171-175}\text{Hf}$ , respectively. By applying these

new adjustments, one could see that the CNSB results are in good agreement with the experiments, although there are still some discrepancies between the theory and experiments, especially at the low spins and at the paired crossing frequencies (which occur a bit lower in the theory). One should also note that these discrepancies cannot be eliminated further by adjusting the parameters and are most probably due to the nature of the applied pairing approach. However, resolving this would be a challenge for further future studies.

- 
- [1] B. Singh, R. Zywna, and R. B. Firestone, *Nucl. Data Sheets* **97**, 241 (2002).
- [2] A. Neußer-Neffgen, H. Hübel, P. Bringel, J. Domscheit, E. Mergel, N. Nenoff, A. K. Singh, G. B. Hagemann, D. R. Jensen, S. Bhattacharya *et al.*, *Phys. Rev. C* **73**, 034309 (2006).
- [3] Y. C. Zhang, W. C. Ma, A. V. Afanasjev, G. B. Hagemann, J. Begnaud, M. P. Carpenter, P. Chowdhury, D. M. Cullen, M. K. Djongolov, D. J. Hartley *et al.*, *Phys. Rev. C* **76**, 064321 (2007).
- [4] M. Djongolov, D. Hartley, L. Riedinger, F. Kondev, R. Janssens, K. A. Saleem, I. Ahmad, D. Balabanski, M. Carpenter, P. Chowdhury *et al.*, *Phys. Lett. B* **560**, 24 (2003).
- [5] D. J. Hartley, W. H. Mohr, J. R. Vanhoy, M. A. Riley, A. Aguilar, C. Teal, R. V. F. Janssens, M. P. Carpenter, A. A. Hecht, T. Lauritsen *et al.*, *Phys. Rev. C* **72**, 064325 (2005).
- [6] D. T. Scholes, D. M. Cullen, F. G. Kondev, R. V. F. Janssens, M. P. Carpenter, D. J. Hartley, M. K. Djongolov, G. Sletten, G. Hagemann, C. Wheldon *et al.*, *Phys. Rev. C* **70**, 054314 (2004).
- [7] R. B. Yadav, W. C. Ma, G. B. Hagemann, H. Amro, A. Bracco, M. P. Carpenter, J. Domscheit, S. Frattini, D. J. Hartley, B. Herskind *et al.*, *Phys. Rev. C* **80**, 064306 (2009).
- [8] W. Koepf and P. Ring, *Nucl. Phys. A* **493**, 61 (1989).
- [9] J. König and P. Ring, *Phys. Rev. Lett.* **71**, 3079 (1993).
- [10] A. Afanasjev, P. Ring, and J. König, *Nucl. Phys. A* **676**, 196 (2000).
- [11] D. Vretenar, A. Afanasjev, G. Lalazissis, and P. Ring, *Phys. Rep.* **409**, 101 (2005).
- [12] T. Bengtsson and I. Ragnarsson, *Nucl. Phys. A* **436**, 14 (1985).
- [13] A. Afanasjev, D. Fossan, G. Lane, and I. Ragnarsson, *Phys. Rep.* **322**, 1 (1999).
- [14] R. Bengtsson, S. Frauendorf, and F.-R. May, *Atom. Data Nucl. Data* **35**, 15 (1986).
- [15] R. Bengtsson and S. Frauendorf, *Nucl. Phys. A* **314**, 27 (1979).
- [16] R. Bengtsson and S. Frauendorf, *Nucl. Phys. A* **327**, 139 (1979).
- [17] M. Wakai and A. Faessler, *Nucl. Phys. A* **295**, 86 (1978).
- [18] H.-L. Ma, B. G. Carlsson, I. Ragnarsson, and H. Ryde, *Phys. Rev. C* **90**, 014316 (2014).
- [19] A. Kardan, I. Ragnarsson, H. Miri-Hakimabad, and L. Rafat-Motevali, *Phys. Rev. C* **86**, 014309 (2012).
- [20] C. M. Petrache, I. Ragnarsson, H.-L. Ma, R. Leguillon, T. Konstantinopoulos, T. Zerrouki, D. Bazzacco, and S. Lunardi, *Phys. Rev. C* **88**, 051303(R) (2013).
- [21] J. Gellanki, B. G. Carlsson, I. Ragnarsson, and D. Rudolph, *Phys. Rev. C* **89**, 024301 (2014).
- [22] B. G. Carlsson, I. Ragnarsson, R. Bengtsson, E. O. Lieder, R. M. Lieder, and A. A. Pasternak, *Phys. Rev. C* **78**, 034316 (2008).
- [23] V. Strutinsky, *Nucl. Phys. A* **95**, 420 (1967).
- [24] G. Andersson, S. Larsson, G. Leander, P. Mller, S. Nilsson, I. Ragnarsson, S. berg, R. Bengtsson, J. Dudek, B. Nerlo-Pomorska *et al.*, *Nucl. Phys. A* **268**, 205 (1976).
- [25] K. Pomorski and J. Dudek, *Phys. Rev. C* **67**, 044316 (2003).
- [26] T. Bengtsson, *Nucl. Phys. A* **496**, 56 (1989).
- [27] C.-H. Yu, G. Hagemann, J. Espino, K. Furuno, J. Garrett, R. Chapman, D. Clarke, F. Khazaie, J. Lisle, J. Mo *et al.*, *Nucl. Phys. A* **511**, 157 (1990).
- [28] D. J. Hartley, W. H. Mohr, J. R. Vanhoy, M. A. Riley, A. Aguilar, C. Teal, R. V. F. Janssens, M. P. Carpenter, A. A. Hecht, T. Lauritsen *et al.*, *Phys. Rev. C* **74**, 054314 (2006).
- [29] J. Recht, Y. Agarwal, K. Blume, M. Guttormsen, H. Hbel, H. Kluge, K. Maier, A. Maj, N. Roy, D. Decman *et al.*, *Nucl. Phys. A* **440**, 366 (1985).
- [30] K. Schmidt, M. Bergström, G. Hagemann, B. Herskind, G. Sletten, P. Varmette, J. Domscheit, H. Hübel, S. Ødegård, S. Frattini *et al.*, *Eur. Phys. J. A* **12**, 15 (2001).
- [31] Y. C. Zhang, Q. A. Ijaz, W. C. Ma, G. B. Hagemann, M. P. Carpenter, P. Chowdhury, D. M. Cullen, M. K. Djongolov, D. J. Hartley, R. V. F. Janssens *et al.*, *Phys. Rev. C* **85**, 064307 (2012).
- [32] E. Selin, S. A. Hjorth, and H. Ryde, *Phys. Scr.* **2**, 181 (1970).
- [33] H. X. Wang, Y. H. Zhang, X. H. Zhou, M. L. Liu, B. Ding, G. S. Li, W. Hua, H. B. Zhou, S. Guo, Y. H. Qiang *et al.*, *Phys. Rev. C* **86**, 044305 (2012).
- [34] B. Fabricius, G. Dracoulis, R. Bark, A. Stuchbery, T. Kibèdi, and A. Baxter, *Nucl. Phys. A* **511**, 345 (1990).
- [35] D. M. Cullen, C. Baktash, M. J. Fitch, I. Frosch, R. W. Gray, N. R. Johnson, I. Y. Lee, A. O. Macchiavelli, W. Reviol, X.-H. Wang *et al.*, *Phys. Rev. C* **52**, 2415 (1995).
- [36] B. Fabricius, G. Dracoulis, T. Kibdi, A. Stuchbery, and A. Baxter, *et al.*, *Nucl. Phys. A* **523**, 426 (1991).
- [37] P. Walker, P. Arve, J. Simpson, G. Hagemann, J. Pedersen, G. Sletten, M. Riley, D. Howe, B. Nyak, J. Sharpey-Schafer *et al.*, *Phys. Lett. B* **168**, 326 (1986).
- [38] G. Dracoulis, C. Fahlander, and A. Byrne, *Nucl. Phys. A* **401**, 490 (1983).
- [39] M. D. Voigt, R. Kaczarowski, H. Riezebos, R. Noorman, J. Bacelar, M. Deleplanque, R. Diamond, and F. Stephens, *Nucl. Phys. A* **507**, 447 (1990).
- [40] J. Nyberg, A. Johnson, M. Carpenter, C. Bingham, L. Courtney, V. Janzen, S. Juutinen, A. Larabee, Z.-M. Liu, L. Riedinger *et al.*, *Nucl. Phys. A* **511**, 92 (1990).